

Feasibility of slepton precision measurements at a muon collider

A. FREITAS

*Department of Physics & Astronomy, University of Pittsburgh,
3941 O'Hara St, Pittsburgh, PA 15260, USA*

Abstract

Detectors at a high-energy muon collider must be protected from the decay products of beam muons by installing shielding material around the beam pipe. In this article, the impact of these blind detector regions on new-physics signatures with invisible final-state particles is shown by studying the production of sleptons, the superpartners of leptons. Special attention is given to large backgrounds from two-photon collisions. It is demonstrated how the influence of these backgrounds can be controlled by implementing suitable cuts or running at two different center-of-mass energies, thus permitting precision measurements of the mass and spin of the sleptons. However, these methods become ineffective for small mass differences between the sleptons and their decay products, and it will be difficult to analyze the slepton signal at a muon collider in this case.

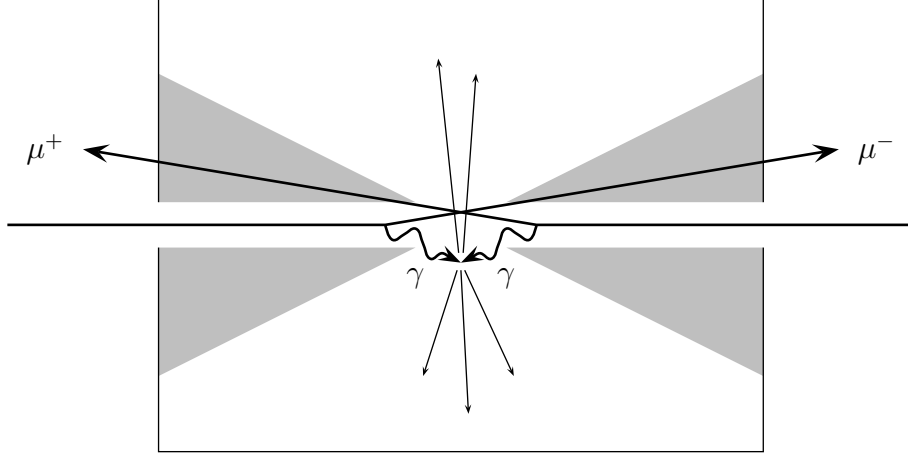


Figure 1: Schematic depiction of conical shielding cones in a MC detector, and a two-photon event with fake missing energy and momentum.

1 Introduction

A high-energy muon collider (MC) is envisaged to be an ideal environment for performing precision measurements in the multi-TeV regime. One major advantage is its sharply defined collision energy, which is only mildly distorted by initial-state radiation, while the influence of beamstrahlung can be completely neglected for most purposes [1]. However, the design of the detector and beam-delivery system will have to account for the large flux of electrons from muon decay inside the beam pipe. The detector can be protected from these decay electrons by installing cone-shaped tungsten shields around the beam pipe near the interaction point. Nevertheless, low-energy secondaries produced in the shielding material may still penetrate the detector, leading to large occupancy values in the inner detector elements. Simulations show that this background can be reduced to acceptable levels by using high-resolution timing information (since secondary particle showers will arrive in the detector with some time delay) and sufficiently massive shielding around the beam pipe*.

However, the absence of instrumentation inside the shielding cones leads to reduced angular coverage of the detector, which can affect the effectiveness of new physics searches and measurements. In particular, physics signatures with missing energy can receive large backgrounds from photon-photon interactions[†]. Here, the photons are radiated off the incident beam muons, which subsequently escape into the blind cone regions, leading to apparent missing energy and momentum, see Fig. 1.

In this paper, the effect of the blind cones on the precision analysis of sleptons, the supersymmetric partners of leptons, is investigated. For concreteness, production of R-smuons $\tilde{\mu}_R$ and R-electrons \tilde{e}_R is considered, and it is assumed that they decay directly to the lightest neutralino $\tilde{\chi}_1^0$, which is assumed to be the lightest supersymmetric particle and

*The reader is referred to the literature for more details [2].

[†]Although it was recognized earlier that the two-photon background is important, see *e.g.* Ref. [3], it has not been considered in pertinent previous studies on this topic [4].

thus stable and invisible to the detector:

$$\mu^+ \mu^- \rightarrow \tilde{\mu}_R^+ \tilde{\mu}_R^- \rightarrow \mu^+ \mu^- \tilde{\chi}_1^0 \tilde{\chi}_1^0, \quad (1)$$

$$\mu^+ \mu^- \rightarrow \tilde{e}_R^+ \tilde{e}_R^- \rightarrow e^+ e^- \tilde{\chi}_1^0 \tilde{\chi}_1^0. \quad (2)$$

It is demonstrated that Standard Model (SM) backgrounds, especially from two-photon interactions, significantly affect the possibility to determine the masses of both the sleptons and the neutralino, as well as the slepton spin. However, it will be shown that by using modified cuts and measurements at different center-of-mass energies, these quantities can still be obtained with high precision, as long as the slepton-neutralino mass difference is large enough.

2 Mass measurement

It is well known that the masses of the sleptons and neutralino in the processes (1) and (2) can be obtained from the endpoints $E_{\min, \max}$ of the energy spectrum of the final-state leptons $\ell = e, \mu$,

$$E_{\min, \max} = \frac{\sqrt{s}}{4} \left(1 - \frac{m_{\tilde{\chi}_1^0}^2}{m_{\tilde{\ell}_R}^2} \right) \left(1 \pm \sqrt{1 - 4m_{\tilde{\ell}_R}^2/s} \right), \quad \begin{aligned} m_{\tilde{\ell}_R}^2 &= s \frac{E_{\min} E_{\max}}{(E_{\min} + E_{\max})^2}, \\ m_{\tilde{\chi}_1^0}^2 &= m_{\tilde{\ell}_R}^2 \left(1 - \frac{2(E_{\min} + E_{\max})}{\sqrt{s}} \right). \end{aligned} \quad (3)$$

To clearly observe both the upper and lower endpoints, the SM background must be reduced to a sufficiently low level. This has been studied in detail for the International Linear Collider (ILC), which is a proposed e^+e^- collider with up to 1 TeV center-of-mass energy [5, 6][‡]. A typical set of cuts, rescaled for a 3 TeV collider, is given by

$$\text{Exactly one } \ell^+ \text{ and one } \ell^- \text{ with } (|\cos \theta_\ell| < 0.95 \quad \text{and } E_\ell > 25 \text{ GeV}), \quad (4)$$

$$\begin{aligned} \text{No other visible object with either } & (|\cos \theta| < 0.95 \quad \text{and } E > 25 \text{ GeV}), \\ \text{or } & (|\cos \theta| < 0.99998 \text{ and } E > 200 \text{ GeV}), \end{aligned} \quad (5)$$

$$(p_{\ell^+} + p_{\ell^-})^2 > (150 \text{ GeV})^2, \quad p_{\text{miss}}^2 > (150 \text{ GeV})^2, \quad (6)$$

$$\cos \theta_{\ell^-} < +0.6, \quad \cos \theta_{\ell^+} > -0.6, \quad (7)$$

$$|\cos(\phi_{\ell^+} - \phi_{\ell^-})| < 0.9, \quad (8)$$

where E_{ℓ^\pm} , p_{ℓ^\pm} , θ_{ℓ^\pm} , and ϕ_{ℓ^\pm} are the energy, momentum, polar angle, and azimuthal angle of the (anti-)lepton, respectively. The cut (4) ensures that two sufficiently energetic oppositely charged leptons are observed in the central detector. For the purpose of the present study, the momenta of photons within a cone of $\Delta R = \sqrt{(\Delta\eta)^2 + (\Delta\phi)^2} < 0.2$ around a lepton are

[‡]Backgrounds from supersymmetry itself will not be considered here, but it has been shown that they can be controlled with a few additional cuts [6, 7].

detector setup	ILC design	6° shielding cone	20° shielding cone
$\tilde{\mu}_R^+ \tilde{\mu}_R^-$	3062	3114	2780
$\mu^+ \mu^-$	0	89	167
$\tau^+ \tau^- \rightarrow \mu^+ \mu^- + X$	0	0	0
$\mu^+ \mu^- \nu \nu$	731	731	684
$\gamma \gamma \rightarrow \mu^+ \mu^- + X$	153	6341	7416
$\tilde{e}_R^+ \tilde{e}_R^-$	460	471	450
$e^+ e^-$	0	2	4
$\tau^+ \tau^- \rightarrow e^+ e^- + X$	0	0	0
$e^+ e^- \nu \nu$	253	253	221
$\gamma \gamma \rightarrow e^+ e^- + X$	135	6095	7242

Table 1: Event numbers for slepton signal and SM backgrounds after selection cuts (4)–(8), for different detector setups. The numbers correspond to the parameters $\sqrt{s} = 3$ TeV, $m_{\tilde{\ell}_R} = 1$ TeV, $m_{\tilde{\chi}_1^0} = 0.6$ TeV, and an integrated luminosity of 1000 fb^{-1} .

added to that lepton’s momentum. A veto (5) is imposed on any other objects either in the central detector or in the low-angle calorimeter (LCAL), which for a typical ILC detector design go down to a polar angle of about 5 mrad [8][§]. The coverage of small polar angles is crucial for rejecting the two-photon background [9]. The requirement (6) reduces background from Z -boson production, while (7) suppresses W -boson background, which predominantly leads to leptons/anti-leptons in the forward/backward region, respectively. Finally, the cut (8) rejects back-to-back event topologies, which mainly stem from W and τ pair production and two-photon collisions.

Results for signal and background event numbers and lepton energy distributions after application of the cuts (4)–(8) are shown in Tab. 1 and Fig. 2 (a,b), for $\sqrt{s} = 3$ TeV, $m_{\tilde{\ell}_R} = 1$ TeV, and $m_{\tilde{\chi}_1^0} = 0.6$ TeV. The signal and backgrounds from direct di-lepton production and $\gamma\gamma$ collisions have been generated with PYTHIA 6.4 [10], while COMPEP 4.5 [11] was used for four-fermion backgrounds, including intermediate resonant single and pair production of W and Z bosons.

Figure 2 (a) shows that for an ILC-like detector, both endpoints of the muon energy spectrum from smuon pair production are clearly visible over the background after cuts. The location of the endpoints agrees with the nominal values $E_{\min} = 122$ GeV and $E_{\max} = 838$ GeV calculated from eq. 3. For selectron pair production, due to the smaller cross section, the signal-to-background ratio is lower, and the extraction of E_{\min} from the data would require a very careful analysis of the background.

The situation changes dramatically for a typical MC detector with an uninstrumented shielding cone around the beam pipe. Two scenarios are considered: a more conservative

[§]In eq. (5) a slightly larger cutoff of 6 mrad is used to make sure that objects emitted with this angle are fully contained in the LCAL.

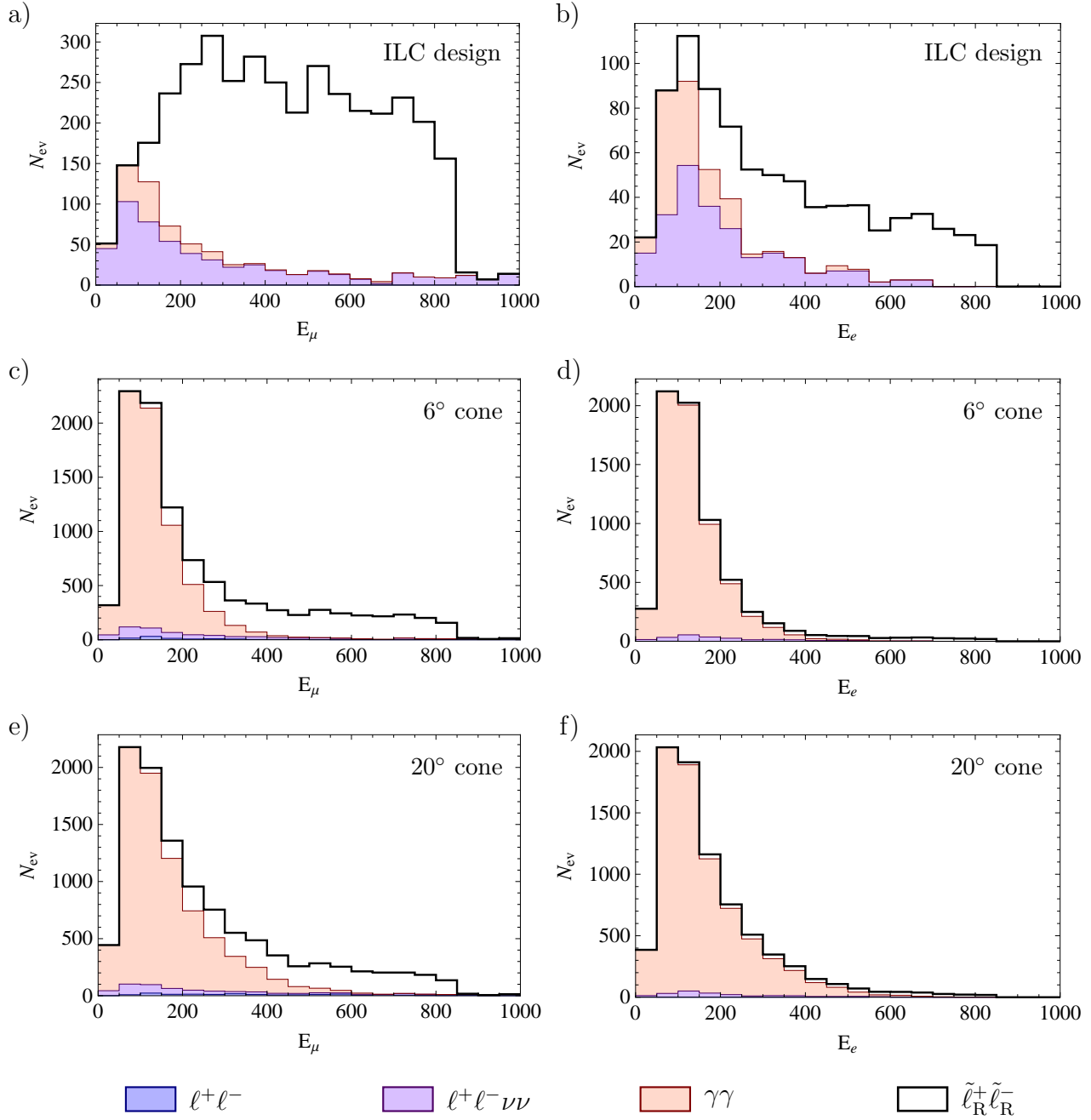


Figure 2: Energy distributions of the final-state leptons after application of the selection cuts (4)–(8) described in the text, for $\tilde{\mu}_R^+ \tilde{\mu}_R^-$ production ($\ell = \mu$, left column) and $\tilde{e}_R^+ \tilde{e}_R^-$ pair production ($\ell = e$, right column). The three rows correspond to different detector setups. The plots are based on the parameters $\sqrt{s} = 3$ TeV, $m_{\tilde{\ell}_R} = 1$ TeV, $m_{\tilde{\chi}_1^0} = 0.6$ TeV, and an integrated luminosity of 1000 fb^{-1} .

detector setup	6° shielding cone	20° shielding cone
$\tilde{\mu}_R^+ \tilde{\mu}_R^-$	1853	1616
$\mu^+ \mu^-$	2	76
$\tau^+ \tau^- \rightarrow \mu^+ \mu^- + X$	0	0
$\mu^+ \mu^- \nu \nu$	364	341
$\gamma \gamma \rightarrow \mu^+ \mu^- + X$	37	243

Table 2: Event numbers for smuon signal and SM backgrounds after selection cuts (4)–(8) and (9), for different detector setups. The numbers correspond to the parameters $\sqrt{s} = 3$ TeV, $m_{\tilde{\mu}_R} = 1$ TeV, $m_{\tilde{\chi}_1^0} = 0.6$ TeV, and an integrated luminosity of 1000 fb^{-1} .

design with a 20° shielding cone, and a very aggressive design with a 6° cone. Due to the lack of angular coverage, the veto cut (5) now only works for objects with scattering angles larger than the cone size, so that a much bigger portion of the two-photon background passes the selection cuts. As can be seen from Tab. 1 and Fig. 2 (c,d,e,f), the signal event rates are completely swamped by the $\gamma\gamma$ background and the lower endpoint of the E_ℓ spectrum is lost in the statistical noise, both for smuon and selectron pair production.

2.1 Analysis strategy using additional cuts

Figure 2 also shows that the two-photon background falls off sharply with increasing lepton energies and essentially disappears for $E_{e,\mu} \gtrsim 400\text{--}500$ GeV. This feature can be used to design a more effective cut for removing the $\gamma\gamma$ background in a MC environment. By demanding that one lepton, here arbitrarily chosen to be the negatively charged one, has an energy above 400 GeV,

$$E_{\ell^-} > 400 \text{ GeV}, \quad (9)$$

the signal-to-background ratio is much improved, see Tab. 2. While this cut obviously eliminates the lower part of the E_{ℓ^-} spectrum, the other lepton, ℓ^+ , can still be used to measure the full lepton energy spectrum with both the upper and lower endpoints $E_{\min, \max}$, see Fig. 3.

In an experimental analysis, the remaining two-photon background after cut (9) may be determined in a data-driven approach from the larger event sample before application of (9), thus reducing the sizeable theoretical uncertainties in the Monte-Carlo simulation of $\gamma\gamma$ collisions. After subtraction of the residual SM background, the ℓ^+ energy spectrum can be fitted by a simple fit function with a sharp cutoff at E_{\min} and E_{\max} . For input parameters $\sqrt{s} = 3$ TeV, $m_{\tilde{\mu}_R} = 1$ TeV, $m_{\tilde{\chi}_1^0} = 0.6$ TeV, and an integrated luminosity of 1000 fb^{-1} , the one-sigma errors from the fit are

$$\text{for } 6^\circ \text{ shielding cone: } \delta m_{\tilde{\mu}_R, \text{fit}} = {}^{+32}_{-40} \text{ GeV}, \quad \delta m_{\tilde{\chi}_1^0, \text{fit}} = {}^{+18}_{-14} \text{ GeV}, \quad (10)$$

$$\text{for } 20^\circ \text{ shielding cone: } \delta m_{\tilde{\mu}_R, \text{fit}} = {}^{+40}_{-46} \text{ GeV}, \quad \delta m_{\tilde{\chi}_1^0, \text{fit}} = {}^{+20}_{-18} \text{ GeV}, \quad (11)$$

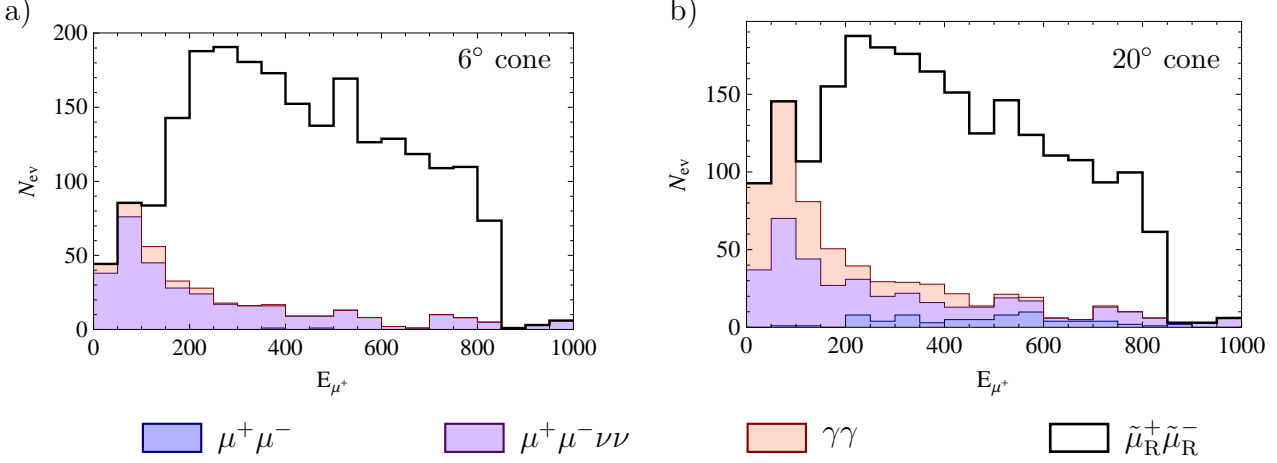


Figure 3: Energy distribution of the μ^+ from $\tilde{\mu}_R^+ \tilde{\mu}_R^-$ production and SM backgrounds, after application of the selection cuts (4)–(8) and (9). Results for a 6° (a) and a 20° (b) shielding cone are shown. The plots correspond to the parameters $\sqrt{s} = 3$ TeV, $m_{\tilde{\mu}_R} = 1$ TeV, $m_{\tilde{\chi}_1^0} = 0.6$ TeV, and an integrated luminosity of 1000 fb^{-1} .

where the numbers reflect statistical uncertainties from the signal and subtracted background. Note that these errors are quite comparable to what one would obtain with an ILC-like detector and *without* the additional cut (9): $\delta m_{\tilde{\mu}_R, \text{ILC}} = {}^{+31}_{-37} \text{ GeV}$, $\delta m_{\tilde{\chi}_1^0, \text{ILC}} = {}^{+17}_{-14} \text{ GeV}$. This seemingly counter-intuitive outcome follows from the fact the mass errors are dominated by the fit of the lower endpoint, whereas the cut (9), in combination with (4)–(8), primarily removes signal events with larger value of E_{ℓ^+} .

2.2 Analysis strategy using two center-of-mass energies

The results of the previous subsection look promising for the case of smuon pair production. For selectrons, on the other hand, the pair production cross section is only about 1/6 of the value for smuons. As a result, even with the cut (9), the lower endpoint of the final-state electron energy spectrum is still obscured by the statistical noise from the remaining SM background.

An alternative strategy, instead of trying to extract both the lower and upper endpoints of the E_ℓ spectrum, is to use only the upper endpoint, but at two different center-of-mass energies \sqrt{s}_1 and \sqrt{s}_2 . From these two measurements one can also uniquely determine the masses of the slepton and of the neutralino,

$$m_{\tilde{\ell}_R}^2 = \frac{E_{\max,1} E_{\max,2} [(E_{\max,1}^2 + E_{\max,2}^2) \sqrt{s_1 s_2} - E_{\max,1} E_{\max,2} (s_1 + s_2)]}{(E_{\max,1}^2 - E_{\max,2}^2)^2}, \quad (12)$$

$$m_{\tilde{\chi}_1^0}^2 = m_{\tilde{\ell}_R}^2 \left[1 + 2 \frac{E_{\max,1}^2 - E_{\max,2}^2}{E_{\max,1} \sqrt{s_1} - E_{\max,2} \sqrt{s_2}} \right], \quad (13)$$

where $E_{\max,1}$ and $E_{\max,2}$ are the upper endpoint energies measured at \sqrt{s}_1 and \sqrt{s}_2 , respectively. This approach also allows one to drop the cut (9), which is only helpful for improving

the signal-to-background ratio at lower energies.

Using simulated events for $\sqrt{s_1} = 2500$ GeV and $\sqrt{s_2} = 3000$ GeV, corresponding to an integrated luminosity of 500 fb^{-1} each, and fitting the upper endpoints of the lepton energy distributions after cuts (4)–(8), one obtains from eqs. (12), (13)

$$\text{for } 6^\circ \text{ shielding cone: } \delta m_{\tilde{\mu}_R, \text{fit}} = {}^{+19}_{-16} \text{ GeV}, \quad \delta m_{\tilde{\chi}_1^0, \text{fit}} = {}^{+8}_{-6} \text{ GeV}, \quad (14)$$

$$\text{for } 20^\circ \text{ shielding cone: } \delta m_{\tilde{\mu}_R, \text{fit}} = {}^{+21}_{-18} \text{ GeV}, \quad \delta m_{\tilde{\chi}_1^0, \text{fit}} = {}^{+9}_{-7} \text{ GeV}. \quad (15)$$

For selectron production, due to the smaller cross section, one obtains somewhat larger errors:

$$\text{for } 6^\circ \text{ shielding cone: } \delta m_{\tilde{e}_R, \text{fit}} = {}^{+49}_{-36} \text{ GeV}, \quad \delta m_{\tilde{\chi}_1^0, \text{fit}} = {}^{+21}_{-13} \text{ GeV}, \quad (16)$$

$$\text{for } 20^\circ \text{ shielding cone: } \delta m_{\tilde{e}_R, \text{fit}} = {}^{+55}_{-32} \text{ GeV}, \quad \delta m_{\tilde{\chi}_1^0, \text{fit}} = {}^{+24}_{-13} \text{ GeV}. \quad (17)$$

It is important, however, to note that this analysis strategy is very robust, since the upper endpoint of the E_ℓ spectrum from $\tilde{\ell}_R^+ \tilde{\ell}_R^-$ production is essentially background-free and thus there are no systematic uncertainties from the background simulation and subtraction.

3 Reach

In the previous section, a scenario with a relatively large mass difference $m_{\tilde{\mu}_R} - m_{\tilde{\chi}_1^0} = 400$ GeV was considered. For smaller mass differences, which are expected in co-annihilation scenarios, the final-state lepton energy spectrum becomes softer. For sufficiently small values of $m_{\tilde{\mu}_R} - m_{\tilde{\chi}_1^0}$, the upper endpoint E_{max} can thus lie in a range with significant SM background levels. In this case, both measurement strategies described in the previous section will be affected by statistical and systematical errors of the background, and a reliable measurement will be impossible when these uncertainties become dominant.

To quantify this problem one needs to define a criterion for the minimum event yield and allowable background level for the endpoint measurement. Here a very simple rule is adopted, demanding that the bins of the energy spectrum near the endpoint must have a signal-to-background ratio of at least one and must contain at least 10 events per bin, for a bin width of 50 GeV (as in the figures above). Using this criterion, the estimated reach of a 3 TeV muon collider is depicted in Fig. 4, for the three cases of an ILC-like detector, a 6° shielding cone, and a 20° shielding cone. The plot has been generated by interpolating between simulated results for a range of smuon and neutralino masses, applying the cuts (4)–(8) in each case.

As evident from the figure, the reach is limited by two factors. On one hand, for smuon masses close to the beam energy the $\tilde{\mu}_R^+ \tilde{\mu}_R^-$ cross section is rather small and thus are affected by the high-energy tail of the residual SM background. On the other hand, for small mass differences $m_{\tilde{\mu}_R} - m_{\tilde{\chi}_1^0}$, the signal E_μ spectrum becomes soft and therefore lies in a kinematic regime with large SM backgrounds. Since the background level grows with increasing blind cone of the detector, the accessible parameter region is reduced in both directions for a MC, compared to a hypothetical multi-TeV ILC-like collider. In particular, it will be difficult to explore co-annihilation scenarios at a MC.

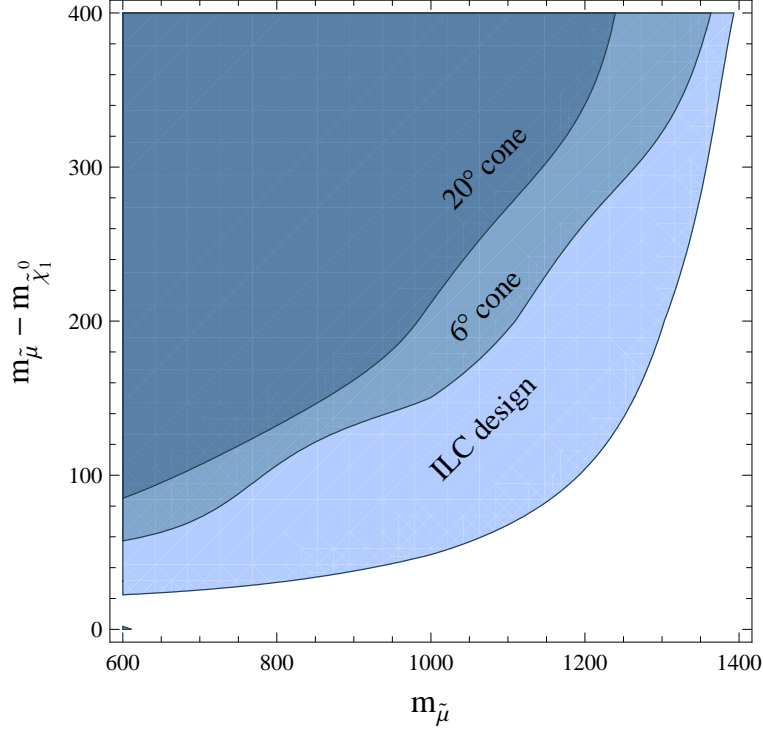


Figure 4: Estimated region of smuon parameter space for which a reliable measurement of the upper endpoint of the E_μ spectrum is possible, for different detector setups. The criterion for what constitutes a reliable measurement is described in the text. The plot corresponds to a muon collider with $\sqrt{s} = 3$ TeV and an integrated luminosity of 1000 fb^{-1} .

Depending on the supersymmetry scenario, however, it may still be possible to obtain a robust $\tilde{\mu}_R$ signal in this case if the smuons are also produced in the decays of heavier superpartners. Such cascade decays can lead to a distinct signal over the SM background as long as the visible decay products are sufficiently energetic, *i.e.* for the mass hierarchy $m_{\tilde{\mu}_R} \ll m_{\tilde{X}} < \sqrt{s}$, where $m_{\tilde{X}}$ is the mass of the heavier superpartner. Since this option is highly model-dependent, it will not be explored further here.

4 Spin determination

While the endpoints of the E_ℓ spectrum are related to the slepton and neutralino masses, the shape of this distribution contains information about the slepton spin. Since sleptons are scalars the E_ℓ distribution is theoretically exactly flat, although in practice the shape is slightly distorted by selection cuts.

As an alternative, let us consider the process

$$\mu^+ \mu^- \rightarrow \tilde{\chi}_1^+ \tilde{\chi}_1^- \rightarrow \ell^+ \tilde{\nu}_\ell \ell^- \tilde{\nu}_\ell^*, \quad (18)$$

where it is assumed that the sneutrinos $\tilde{\nu}_\ell^{(*)}$ decay invisibly [12]. In this case, the primary pair-produced particles (the charginos $\tilde{\chi}_1^\pm$) are fermions. For this process, the E_ℓ distribution

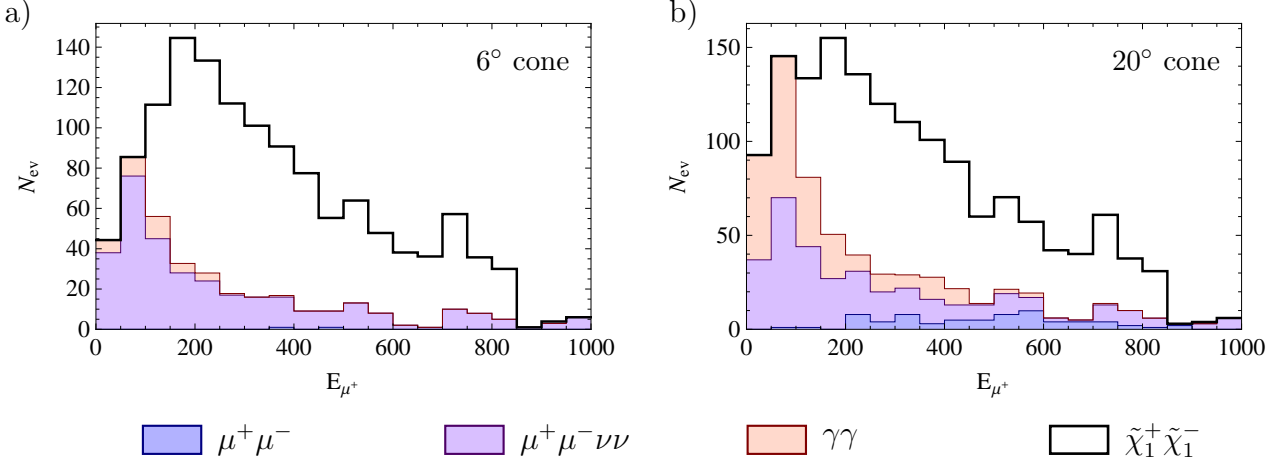


Figure 5: Muon energy distribution from $\tilde{\chi}_1^+\tilde{\chi}_1^-$ production and SM backgrounds, after application of the selection cuts (4)–(8) and (9). Results for a 6° (a) and a 20° (b) shielding cone are shown. The plots correspond to the parameters $\sqrt{s} = 3$ TeV, $m_{\tilde{\chi}_1^\pm} = 1$ TeV, $m_{\tilde{\nu}_\mu} = 0.6$ TeV, and an integrated luminosity of 1000 fb^{-1} .

is not flat, but spin correlations lead to a relative accumulation of events near the lower end, see Fig. 5.

In general, the $\tilde{\chi}_1^+\tilde{\chi}_1^-$ production cross section is different from the $\tilde{\mu}_R^+\tilde{\mu}_R^-$ and $\tilde{e}_R^+\tilde{e}_R^-$ cross section, and this fact may also be employed to distinguish these processes. However, the observable production rate also depends on other model-dependent factors such as branching fractions. In this work, therefore, only the shape information of the E_ℓ distribution will be used for spin discrimination, and the signal distribution in Fig. 5 has been rescaled to match the generator-level cross section for $\tilde{\mu}_R^+\tilde{\mu}_R^-$ production.

Since the distinctive feature between scalars and fermion is the absence or presence of an accumulation near the lower end of the E_ℓ distribution, it is important to observe the whole E_ℓ spectrum, not only the upper endpoint. To sufficiently reduce the SM backgrounds, one thus has to use the selection cut (9) in addition to (4)–(8). Results for $\ell = \mu$ are shown in Fig. 3 for scalars and Fig. 5 for fermions.

The discriminative power between the two spin scenarios can be illustrated with a simple binned χ^2 test, applied to the range 200–1000 GeV of the E_μ distribution. By demanding a lower limit of 200 GeV, the $\gamma\gamma$ background becomes subdominant, and the remaining SM background components can be computed reliably from Monte-Carlo simulations. In the fit, the overall normalization has been left free-floating. Assuming a total luminosity of 1000 fb^{-1} , the scalar and fermion scenarios can be distinguished with a statistical significance of 7.7 standard deviations for a 6° blind cone and 6.0 standard deviations for a 20° blind cone.

Note, however, that the spin determination is much more difficult or even practically impossible for smaller mass differences $\Delta m = (m_{\tilde{\mu}_R} - m_{\tilde{\chi}_1^0})$, $(m_{\tilde{\chi}_1^\pm} - m_{\tilde{\nu}})$, since in this case the separation of signal and SM backgrounds becomes problematic, as discussed in section 3. In particular, the cut (9) will entirely remove all signal events for small values of Δm .

5 Conclusions

At a future muon collider, the analysis of new-physics signatures with missing energy is substantially impacted by the presence of uninstrumented shielding cones around the beam pipe in the detector. Most notably, the limited angular coverage of the detector leads to large backgrounds from two-photon collisions. In this article, this problem has been studied in detail by considering the pair production of sleptons, supersymmetric partners of leptons, as an example. It was found that the potential for accessing this signal depends essentially on the mass difference Δm between the sleptons and their decay products, which here are assumed to be stable neutralinos.

For relatively large mass differences, $\Delta m \gtrsim \mathcal{O}(100 \text{ GeV})$, the two-photon and other Standard Model backgrounds can be reduced by suitable selection cuts, which allows one to clearly identify the new-physics signal and determine properties such as slepton spin. Furthermore, by taking data at two different center-of-mass energies, the masses of both the sleptons and their decay products can be measured with percent-level precision.

On the other hand, for small slepton-neutralino mass differences, it becomes difficult to robustly separate the photon-photon background from the signal. The large background levels can make it impossible to determine the slepton masses and spins or even establish a discovery of the signal in this case. In consequence, the reach for new-physics signatures with small Δm is more limited at a muon collider compared to an e^+e^- collider. However, it would still be possible to analyze slepton production and decay in such a scenario at a muon collider if one can take advantage of cascade decays of heavier superpartners into the sleptons.

Interestingly, it turns out that the size of the blind shielding cones has only a mild influence on these results, even when comparing two extreme scenarios: a very optimistic case with a 6° shielding cone, and a conservative case with a 20° shielding cone.

Acknowledgements

This project was supported in part by the National Science Foundation under grant PHY-0854782.

References

- [1] For a recent summary, see *e.g.* V. Shiltsev, *Mod. Phys. Lett. A* **25**, 567 (2010).
- [2] S. Kahn, contribution to the *Low-Emittance Muon Collider Workshop, Fermilab, Batavia, IL (2006)*, http://www.muonsinc.com/mcwfeb06/presentations/SKahn_02072006_DetectorBackgroundsLEMC.pdf;
N. V. Mokhov, Y. I. Alexahin, V. V. Kashikhin, S. I. Striganov and A. V. Zlobin, contribution to the *2011 Particle Accelerator Conference (PAC'11), New York, NY (2011)*, FERMILAB-CONF-11-094-APC;

- S. A. Kahn, M. A. C. Cummings, T. J. Roberts, A. O. Morris, D. Hedin and J. Kozminski, contribution to the *2011 Particle Accelerator Conference (PAC'11)*, New York, NY (2011), PAC-2011-THPO88.
- [3] J. C. Gallardo *et al.*, “Muon-Muon Collider: A Feasibility Study,” in *The Proceedings of 1996 DPF/DPB Summer Study on New Directions for High-Energy Physics (Snowmass 96)*, Snowmass, CO, chapt. 9;
M. Klasen, AIP Conf. Proc. **435**, 495 (1998).
 - [4] D. Greenwald and A. Caldwell, contribution to the *2011 Particle Accelerator Conference (PAC'11)*, New York, NY (2011), PAC-2011-MOP018.
 - [5] K. Hidaka, H. Komatsu and P. Ratcliffe, Nucl. Phys. B **304**, 417 (1988);
T. Tsukamoto, K. Fujii, H. Murayama, M. Yamaguchi and Y. Okada, Phys. Rev. D **51**, 3153 (1995);
A. Freitas, A. von Manteuffel and P. M. Zerwas, Eur. Phys. J. C **34**, 487 (2004).
 - [6] H.-U. Martyn, in *Conceptual Design of a 500 GeV e^+e^- Linear Collider*, eds. R. Brinkmann, G. Materlik, J. Rossbach and A. Wagner, DESY 1997-048 and ECFA 1997-182.
 - [7] A. Freitas, D. J. Miller and P. M. Zerwas, Eur. Phys. J. C **21**, 361 (2001).
 - [8] T. Abe *et al.* [ILD Concept Group – Linear Collider Collaboration], FERMILAB-LOI-2010-03, arXiv:1006.3396 [hep-ex].
 - [9] H. U. Martyn, in *Proc. of the International Conference on Linear Colliders (LCWS 04)*, Paris, France, 19-24 Apr 2004 [arXiv:hep-ph/0408226].
 - [10] T. Sjöstrand, S. Mrenna and P. Z. Skands, JHEP **0605**, 026 (2006).
 - [11] E. Boos *et al.* [CompHEP Collaboration], Nucl. Instrum. Meth. A **534**, 250 (2004).
 - [12] A. Freitas, W. Porod and P. M. Zerwas, Phys. Rev. D **72**, 115002 (2005).